Proceedings of the ASME 2018 International Design Engineering Technical Conferences & Computers and Information in Engineering Conference
IDETC/CIE 2018
August 26-29, 2018, Quebec City, Quebec, Canada

DETC2018-85248

PROGRAMMABLE CONSTANT-FORCE MULTISTABLE MECHANISMS

Mohamed Zanaty*
Instant-lab
Ecole Polytechnique Fédérale de Lausanne (EPFL)
Neuchâtel 2002, Switzerland
Email: mohamed.zanaty@epfl.ch

Simon Henein
Instant-lab
Ecole Polytechnique Fédérale de Lausanne (EPFL)
Neuchâtel 2002, Switzerland
Email: simon.henein@epfl.ch

ABSTRACT

Programmable multistable mechanisms exhibit stability behavior whereby the stiffness and the number of stable states can be controlled via programming inputs. In this paper, we report the zero stiffness behavior of a 2-degree of programming (DOP) T-combined, axially loaded double parallelogram multistable mechanism. We demonstrate zero force monostability, constant force monostability, zero force bistability, constant force bistability and zero force tristability behaviors by tuning the programming input. We derive analytically the reaction force of the mechanism for each configuration and verify our analytical results using numerical simulations and experimental measurements, showing less than 10% *discrepancy. The concept of constant-force programming can be extended to N-DOP T-combined, serial combined and parallel combined programmable multistable mechanisms. Finally, we present potential applications of stability programming.*

1 Introduction

Compliant mechanisms are mechanical devices that perform their function through the bending of their flexural elements. They can exhibit negative and zero stiffness behaviors affecting the mechanism stability, such as constant force mechanisms (CFMs) [1] and multistable mechanisms [2]. CFMs exhibit a near zero stiffness (ZS) within a certain range of their stroke and are applied in micro-manipulation of sensitive objects such as medical operations and micro-assembly [3]. Examples of CFMs are elastically loaded nonuniform cams [4]. Parallel combinations of bistable springs with positive-stiffness spring can lead to constant-force response [5]. Special shapes of curved beams can exhibit zero stiffness response as discussed in [6]. Morsch [7] and Merriam [8] reported a constant torque mechanism combining compliant cross pivots with preloaded springs. However, all these mechanisms are monostable, i.e., they have only one stable state.

Multistable mechanisms have more than one stable state within their range of motion. They are characterized by the stiffness and position of their equilibrium states and their degree of stability *(DOS)*, which represents the number of stable states [9–11]. They have a wide range of applications such as mechanical switching [12] and energy harvesting [13]. Combining multistability with ZS enables new applications such as force regulation demonstrated by the constant force bistable mechanism - DOS =2, in [14].

In this paper, we study the stiffness behavior of programmable multistable mechanisms (PMMs), which demonstrate combined programmable ZS and multistability behaviors. We report analytically, numerically and experimentally for the first time the zero force monostability, constant force monostability, zero force bistability, constant force bistability and zero force tristability of the T-shaped mechanism, an example of PMMs. This can bring new applications such as tunable constant force grippers and programmable force regulators. PMMs were introduced in the authors' previous work [15, 16] in which the DOS,

*Address all correspondence to this author.

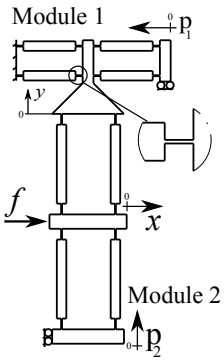

FIGURE 1. T-shaped mechanism based on double parallelogram mechanisms with rectangular hinges.

the stiffness and the position of the stable states of the mechanism are modified by external inputs, known as *programming input*. In the case of the T-shaped mechanism, the stability behavior can switch between monostability, bistability, tristability, and quadrastability.

The paper is organized as follows. Firstly, we introduce the operation of the T-shaped mechanism and possible stability and stiffness behaviors. We calculate the reaction force based on Euler Bernoulli equations and represent it as a seventh order polynomial and the stiffness as a sixth order polynomial from which the stability and stiffness behaviors are characterized. We verify our analysis using finite element analysis and experimental measurements. Finally, we present potential applications of PMMs.

2 T-shaped mechanism

The T-shaped mechanism consists of two orthogonally combined modules in a way similair to [17], as illustrated in Figure 1. Each module is an axially loaded double parallelogram mechanism consisting of eight rectangular hinges monolithically connected by rigid links. Module 1 is fixed on one extremity and axially guided on the other extremity by the programming input, p_1. Module 2 is guided on one extremity by the programming input p_2 and the other extremity is connected to the central block of module 1 in the lateral direction of the module 1 beams. The actuation input x is applied to the central block of module 2 in the lateral direction of its beams.

Stability behavior of the mechanism depends on p_1 and p_2, as we illustrated previously [16]. We define p_1^{cr} as the minimum value of p_1 at which module 1 buckles with sufficient lateral force to buckle module 2 and p_2^c as the maximum value of p_2 at which module 2 exhibits zero stiffness around $x = 0$.

If $p_1 < p_1^{cr}$, the mechanism is either monostable for $p_2 < p_2^c$ or bistable for $p_2 > p_2^c$. For $p_1 > p_1^{cr}$, module 1 buckles and it has three equilibrium states at $y = p_2^a, p_2^b, p_2^c$, where $p_2^a < p_2^b < p_2^c$. Stable states occur at p_2^a, p_2^c and unstable state at p_2^b. If $p_2 < p_2^a$, the mechanism is monostable as module 1 does not reach either of its stable states. For $p_2^b > p_2 > p_2^a$, module 1 surpasses a stable state and the mechanism is bistable. If $p_2^c > p_2 > p_2^b$, module 1 surpasses its unstable state and the mechanism exhibits tristability. For $p_2 > p_2^c$, module 1 surpasses both of its stable states and the mechanism is quadrastable [15]. Table 1 summarizes the conditions of the programming inputs, illustrating the stable states of the T-mechanism for each region.

TABLE 1. Stable states for each stability region and their programming conditions.

Stable states	DOS	p_1	p_2
q_0 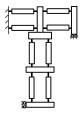	1	$p_1 < p_1^{cr}$	$p_2 < p_2^c$
		$p_1 > p_1^{cr}$	$p_2 < p_2^a$
q_1^-, q_1^+ 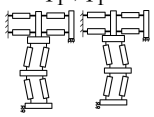	2	$p_1 < p_1^{cr}$	$p_2 > p_2^c$
q_3^-, q_3^+ 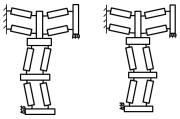	2	$p_1 > p_1^{cr}$	$p_2^a < p_2 < p_2^b$
q_3^-, q_0, q_3^+ 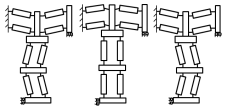	3	$p_1 > p_1^{cr}$	$p_2^b < p_2 < p_2^c$
$q_3^-, q_1^-, q_1^+, q_3^+$ 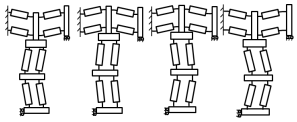	4	$p_1 > p_1^{cr}$	$p_2 > p_2^c$

The T-mechanism exhibits zero stiffness within a certain range of its stroke as it switches its DOS, behaving as *programmable constant force mechanism* as illustrated in Figure 2. On fixing p_1 such that $p_1 > p_1^{cr}$ and changing p_2, the mechanism is zero force monostable (ZFMM) at $p_2 = p_2^a$, where the mechanism switches from monostability to bistability. The mechanism is zero force bistable (ZFBM) at $p_2 = p_2^b$, where the mechanism switches from bistability to tristability and zero force tristable (ZFTM) at $p_2 = p_2^c$ for $p_1 > p_1^{cr}$ where the mechanism switches from tristability to quadrastability.

On selecting $p_2^b < p_2 < p_2^c$ and sweeping p_1, the mechanism shows zero stiffness region and behaves as a constant force

TABLE 2. Zero stiffness behavior as a function of programming inputs and their DOS.

ZS Behavior	Conditions	DOS Localization
ZFMM	$p_2 = p_2^c,\ p_1 < p_1^{cr}$	Boundary $1-2$
ZFMM	$p_2 = p_2^a$	Boundary $1-2$
CFMM	$p_1 = p_1^z,\ p_2 < p_2^c$	Region 1
ZFBM	$p_2 = p_2^b$	Boundary $2-3$
CFBM	$p_1 = p_1^z,\ p_2 > p_2^c$	Region 2
ZFTM	$p_2 = p_2^c,\ p_1 > p_1^{cr}$	Boundary $3-4$

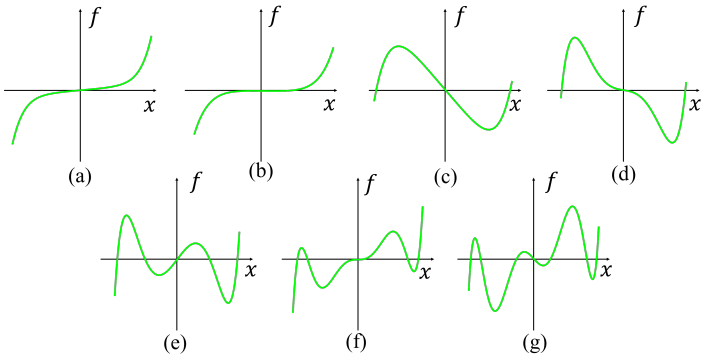

FIGURE 2. Reaction force of the mechanism as it evolves from monostability to bistability to tristability to quadrastability on sweeping p_2 for $p_1 > p_1^{cr}$, (a) monostable, (b) ZFMM, (c) bistable, (d) ZFBM, (e) tristable, (f) ZFTM, (g) quadrastable.

monostable mechanism (CFMM) as it switches from monostability to tristability, given in Figures 3(a), (b), (c). Similarly, for $p_2 > p_2^c$, the mechanism exhibits zero stiffness response on switching from bistability to quadrastability and it is a constant force bistable mechanism (CFBM) as shown in Figures 3(d), (e), (f).

Table 2 summarizes the different zero stiffness (ZS) behaviors of the T-mechanism as a function of the programming inputs and DOS localization. We denote the value of p_1 at which the mechanism exhibits zero stiffness response for a given value of p_2 as p_1^z. It should be noted that

1. The value p_1^{cr} depends only on the dimensions of the mechanism.
2. The values, p_2^a, p_2^b, p_2^c are functions of p_1.
3. The values, p_2^a, p_2^b exist only for $p_1 > p_1^{cr}$.
4. The value p_1^z is a function of p_2.

Figure 4 shows the T-mechanism discussed in this paper with its main dimensions given in Table 3. A programming spring with stiffness k_r is used to axially load module 1. The

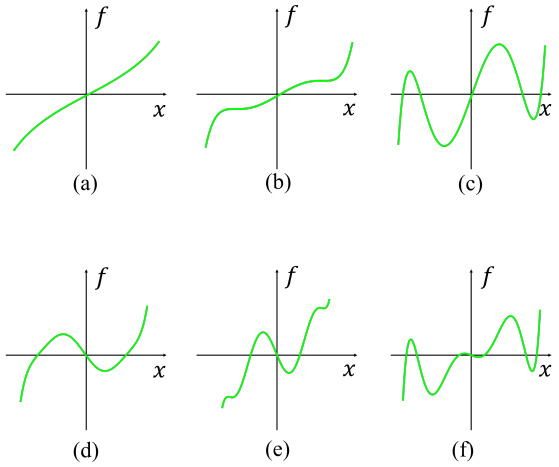

FIGURE 3. Reaction force of the mechanism as it evolves from monostability to tristability, on sweeping p_1 for $p_2^b < p_2 < p_2^c$ (a) monostable, (b) CFMM, (c) tristable, and from bistability to quadrastability for $p_2 > p_2^c$, (d) bistable, (e) CFBM, (f) quadrastable.

central block of module 2 is replaced by two rigid blocks connected by two pivots to avoid kinematic over constraints [16].

The reaction force f depends on the lateral stiffness ratio between module 1 to the programming spring, the lateral stiffness ratio of module 2 to module 1 and beam length ratio which we denote as η_1, η_2, α_2, respectively.

$$\eta_1 = \frac{I_1 \ell_r^3}{I_r \ell_1^3}, \quad \eta_2 = \frac{I_2 \ell_1^3}{I_1 \ell_2^3}, \quad \alpha_2 = \frac{\ell_2}{\ell_1} \tag{1}$$

where $I_1 = wt_1^3/12$, $I_2 = wt_2^3/12$, $I_r = wt_r^3/12$. We define the parameters, Γ_1, Γ_2, Ψ_1, Ψ_2 to represent the effect of the rigid links [18].

$$\begin{aligned}
\Gamma_1 &= \frac{1}{2a_{01}(3-6a_{01}+4a_{01}^2)}, \quad \Gamma_2 = \frac{1}{2a_{02}(3-6a_{02}+4a_{02}^2)} \\
\Psi_1 &= \frac{15-50a_{01}+60a_{01}^2-24a_{01}^3}{2(3-6a_{01}+4a_{01}^2)^2}, \\
\Psi_2 &= \frac{15-50a_{02}+60a_{02}^2-24a_{02}^3}{2(3-6a_{02}+4a_{02}^2)^2}
\end{aligned} \tag{2}$$

where

$$a_{01} = \frac{c_1}{\ell_1}, \quad a_{02} = \frac{c_2}{\ell_2}.$$

TABLE 3. Dimensions of the T-mechanism

Parameter	Description	Theortical	Measured
w	Beam Width	10 [mm]	10[mm]
Programming spring			
ℓ_r	Beam length	15[mm]	15[mm]
t_r	Beam thickness	350[μm]	345[um]
Module 1			
ℓ_1	Beam length	23[mm]	
t_1	Hinge thickness	80[um]	78[μm]
c_1	Hinge length	4.0[mm]	3.9[mm]
Module 2			
ℓ_2	Beam length	36[mm]	
t_2	Hinge thickness	50[μm]	49[μm]
c_2	Hinge length	3[mm]	2.9[mm]

3 Analytical model

We applied Euler Bernoulli equations to model the reaction force of the mechanism and we assume that:

1. A linear elastic material is used with Young's modulus Y.
2. The forces of module 1 are normalized by EI_1/ℓ_1^2 and its displacement by ℓ_1 and forces of module 2 are normalized by EI_2/ℓ_2^2 and its displacement by ℓ_2.
3. The beams of the mechanism are slender enough that their shear strain is ignored.
4. The beams of the mechanism do not buckle for second or higher order buckling modes.
5. The axial load of the programming spring is negligible compared to its buckling load.
6. The beams of the mechanism deform within their intermediate range of motion.

Our model is based on calculating the relation between applied actuation displacement x and axial displacements λ_1 and λ_2. After that, we calculate the axial loads of module 1 and module 2, represented as N_1 and N_2, respectively as illustrated in Figure 4. Then, using the secant stiffness of module 2, the reaction force of the mechanism is represented as seventh order polynomial [15]:

$$\hat{f} = \frac{f\ell_2^2}{EI_2} = \hat{x}\Phi(\hat{x}^2) \tag{3}$$

where

$$\Phi(z) = \beta_0 + \beta_1 z + \beta_2 z^2 + \beta_3 z^3 \tag{4}$$

and

$$\begin{aligned}
\beta_0 &= \frac{48}{\Gamma_2} - \frac{576\Psi_2\eta_2}{5\Gamma_1}\hat{p}_2 + \frac{3456\eta_1\eta_2\Psi_1\Psi_2}{25}\hat{p}_1\hat{p}_2 \\
&\quad - \frac{20736\eta_1\eta_2\Psi_1^2\Psi_2\alpha_2^2}{125}\hat{p}_2^3, \\
\beta_1 &= \frac{3456\eta_2\Psi_2^2}{25\Gamma_1} - \frac{20736\eta_1\eta_2\Psi_1\Psi_2^2\hat{p}_1}{125}, \\
&\quad + \frac{373248\alpha_2^2\eta_1\eta_2\Psi_1^2\Psi_2^2\hat{p}_2^2}{625} \\
\beta_2 &= \frac{-2239488\alpha_2^2\eta_1\eta_2\Psi_1^2\Psi_2^3\hat{p}_2}{3125}, \\
\beta_3 &= \frac{4478976\alpha_2^2\eta_1\eta_2\Psi_1^2\Psi_2^4}{15625},
\end{aligned} \tag{5}$$

where $\hat{x} = x/\ell_2$, $\hat{p}_1 = p_1/\ell_1$ and $\hat{p}_2 = p_2/\ell_2$. The stability behavior of the mechanism can be extracted from the polynomial $\Phi(z)$ where

1. DOS can be calculated using Descartes rule of sign from sign alternation of the coefficients $\beta_0, \beta_1, \beta_2, \beta_3$ and the sign of Δ_ϕ, the discriminant of $\Phi(z)$ as illustrated in Figure 5(a), (b), (c) [15].
2. The position of equilibrium states are the square roots of z_i^q, positive-valued zeros of $\Phi(z)$,

$$\hat{q}_0 = 0, \quad \hat{q}_i^{\pm} = \pm\sqrt{z_i^q}, \quad i = 1,2,3. \tag{6}$$

3. The value p_1^{cr} is the value of p_1 at which the discriminant of $\phi(z)$ is zero [16],

$$\hat{p}_1^{cr} = \frac{p_1^{cr}}{\ell_1} = \frac{5}{6\Gamma_1\eta_1\eta_2} + \frac{126}{127}\Big(\frac{\alpha_2^2}{\eta_1^2\eta_2^2\Gamma_2^2\Psi_1\Psi_2^2}\Big)^{1/3} \tag{7}$$

4. The values of $\hat{p}_2^a$, $\hat{p}_2^b$, $\hat{p}_2^c$ are the zeros of β_0.

The tangential stiffness is the first derivative of the reaction force f with respect to its displacement x.

$$\hat{k} = \frac{k\ell_2^3}{EI_2} = \frac{\partial\hat{f}}{\partial\hat{x}} \tag{8}$$

This is represented as sixth order polynomial such that

$$\hat{k} = \kappa(\hat{x}^2) \tag{9}$$

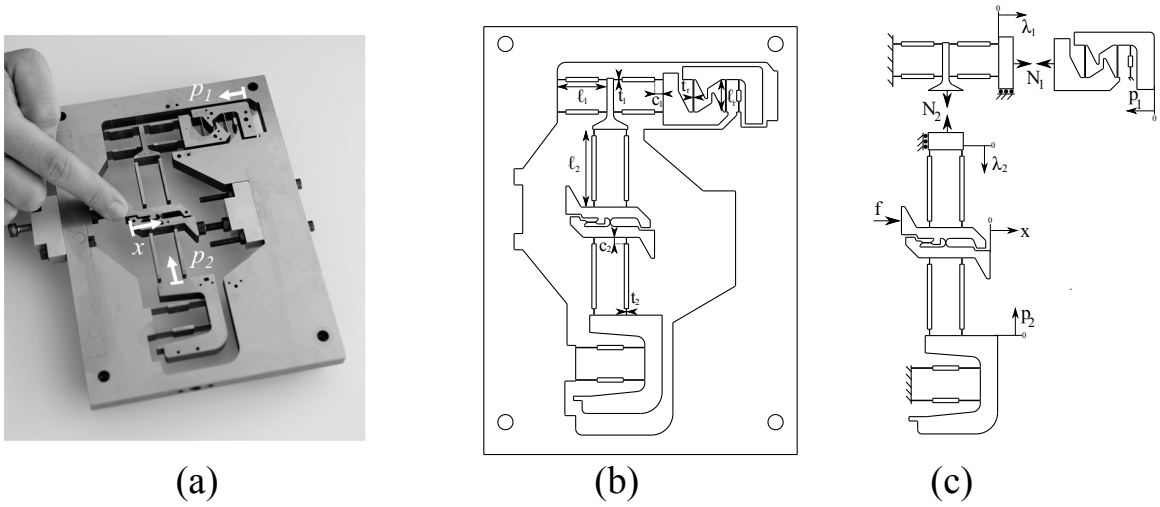

(a) (b) (c)

FIGURE 4. (a) Programmable T-shaped mechanism with programming inputs p_1, p_2 and actuation input x, (b) dimensions of the mechanism, (c) forces and displacements.

where

$$\kappa(z) = \beta_0 + 3\beta_1 z + 5\beta_2 z^2 + 7\beta_1 z^3 \tag{10}$$

Similarly, we can extract the stiffness behavior of the mechanism from the polynomial $\kappa(z)$ such that

1. The number of zero stiffness states can be calculated using the number of sign changes of coefficients $\beta_0, \beta_1, \beta_2, \beta_3$ and the sign of Δ_κ, the discriminant of κ as illustrated in Figure 5(b), (d), (e).
2. The zero stiffness positions are the square roots of z_i^κ, the positive-valued zeros of $\kappa(z)$ where

$$\zeta_i^{\pm} = \pm\sqrt{z_i^\kappa}, \quad i = 1,2,3. \tag{11}$$

3. The value of p_1^z is the zero of Δ_κ, the discriminant of κ.

Figure 6 shows the zero stiffness boundaries, $p_1^{cr}, p_1^z, p_2^a, p_2^b, p_2^c$ and the selected points given in Table 4 that we study in the next section.

4 Results and discussion

The values of the programming inputs, p_1, p_2 determine the stability and stiffness behavior of the T-mechanism. In this section, we discuss the zero stiffness behavior for different DOS based on the calculated reaction force and tangential stiffness from equations (3) and (9), at the points highlighted in Figure 6.

TABLE 4. Selected points for the analysis of the zero stiffness behavior of the T-shaped mechanism.

Points	$p_1[mm]$	$p_2[mm]$	Points	$p_1[mm]$	$p_2[mm]$
a	-0.2	0.6	b	0.0	1.2
c	0.23	0.0	d	0.27	-0.5
e	0.35	-0.8	f	0.4	-0.6
g	0.14	2	h	0.125	2.5
i	0.35	2.65	j	0.4	2.8

We define the zero stiffness region as the range of the displacement x for which the force varies by $\pm 5\%$ and the zero force region as the range of x for which the strain energy remains within $\pm 5\%$.

4.1 Zero force monostable mechanism (ZFMM)

The mechanism is monostable for $p_2 < p_2^a$ or for $p_2 < p_2^c$ and $p_1 < p_1^{cr}$. At $p_2 = p_2^c$ or $p_2 = p_2^a$, the mechanism exhibits a zero stiffness regime around $x = 0$. On changing the value of p_1, the values of p_2^a, p_2^c change and the stiffness of the mechanism beyond the zero stiffness region changes as well. Figure 7 illustrates the reaction force of the mechanism for points (a), (b).

4.2 Constant force monostable mechanism (CFMM)

The mechanism is monostable for $p_1 < p_1^{cr}$ and $p_2 < p_2^c$. At $p_1 = p_1^z$, the mechanism exhibits a constant force regime. The value of the force depends on p_2. As p_2 decreases, p_1^z increases and the value of the constant force decreases and its range in-

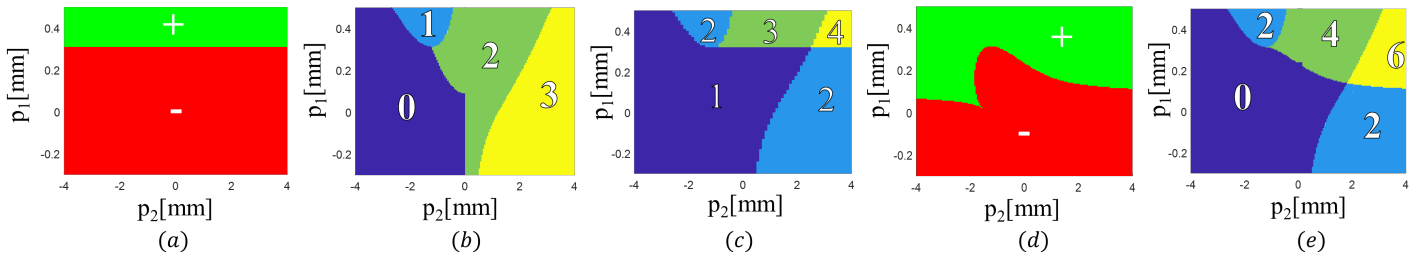

FIGURE 5. (a) Sign of the discriminant of the reaction force polynomial , Δ_Φ, (b) Number of sign alternation of the coefficients β_0, β_1, β_2, β_3, (c) Number of stable states, DOS, (d) Sign of the discriminant of the stiffness polynomial, Δ_κ, (e) Number of zero stiffness states.

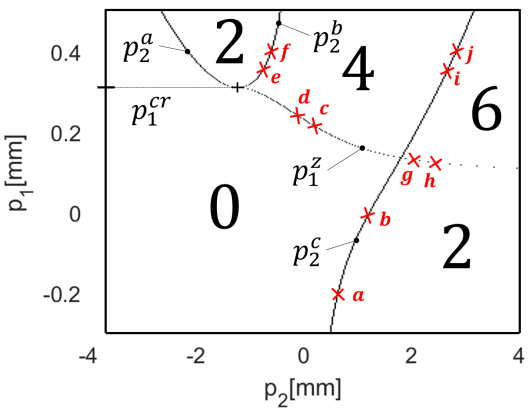

FIGURE 6. Zero stiffness boundaries of the T-mechanism as a function of the programming inputs highlighting our analysis points.

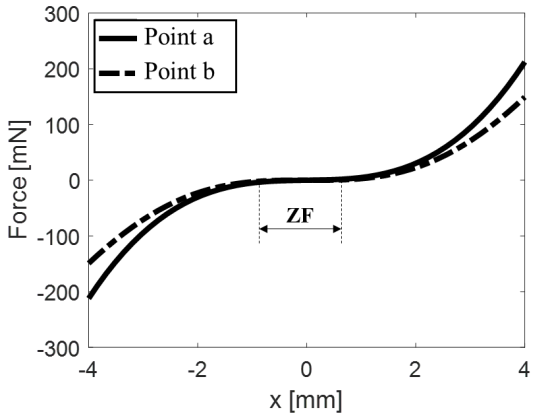

FIGURE 7. The reaction force of the mechanism programmed as ZFMM, the zero force (ZF) region is highlighted.

creases. Decreasing p_2 decreases the stiffness of the mechanism around its equilibrium position as illustrated in Figure 8 for points (c), (d).

4.3 Zero force bistable mechanism (ZFBM)

The mechanism is bistable for $p_1 > p_1^{cr}$ and $p_2^a < p_2 < p_2^b$. At $p_2 = p_2^b$, the mechanism exhibits a zero stiffness response around $x = 0$. On increasing p_1, the value of p_2^b increases and the stiffness around the stable states increases as illustrated in Figure 9 for points (e), (f).

4.4 Constant force bistable mechanism (CFBM)

The mechanism is bistable for $p_1 < p_1^{cr}$ and $p_2 > p_2^c$. At $p_1 = p_1^z$, the mechanism is a constant force bistable as it exhibits a zero stiffness regime. As p_2 increases, the value of p_1^z decreases slightly and the stiffness around equilibrium positions increases. The range of the constant stiffness regime decreases with increasing p_2 as illustrated in Figure 10 for points (g), (h).

4.5 Zero force tristable mechanism (ZFTM)

The mechanism is tristable for $p_1 > p_1^{cr}$ and $p_2^b < p_2 < p_2^c$. At $p_2 = p_2^c$, the mechanism exhibits near zero stiffness around $x = 0$ and becomes a zero force tristable mechanism. On increasing p_1, p_2^c increases and the stiffness at equilibrium states increases as illustrated in Figure 11 for points (i), (j).

5 Zero stiffness and equilibrium positions

We calculated the positions of the near-zero stiffness and equilibrium regions from the stiffness polynomial κ and force polynomials Φ, they are the square roots of the positive-valued zeros as given in equations(11), (6), respectively.

The zero stiffness positions and equilibrium positions are functions of the programming inputs, p_1, p_2. We fix one programming input and change the other one to study the impact of the programming inputs on the stiffness and stability behaviors.

5.1 Sweeping p_1 and fixing p_2

Figure 12 illustrates the variation of zero stiffness and equilibrium positions as a function of p_1 for different values of p_2.

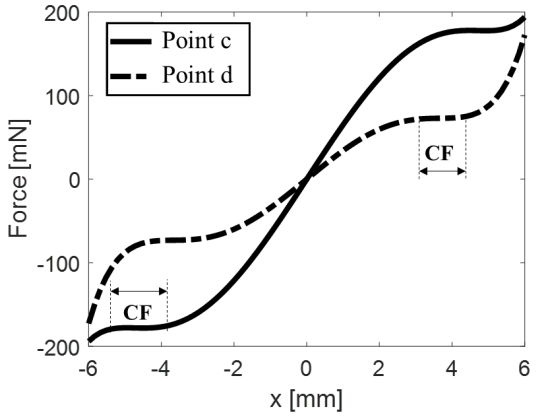

FIGURE 8. The reaction force of the mechanism programmed as CFMM, , the constant force (CF) region is highlighted.

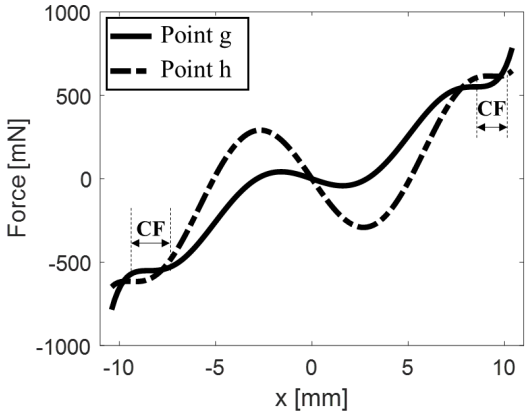

FIGURE 10. The reaction force of the mechanism programmed as CFBM, the constant force (CF) region is highlighted.

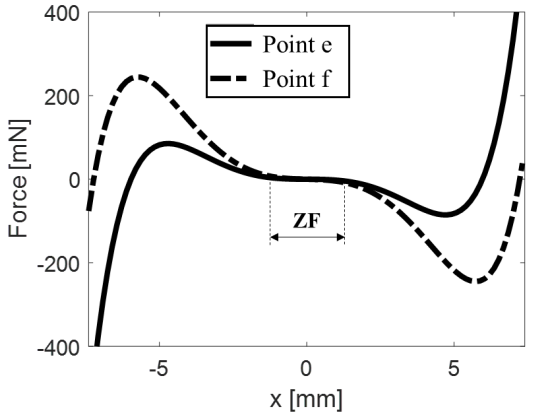

FIGURE 9. The reaction force of the mechanism programmed as ZFBM, the zero force (ZF) region is highlighted.

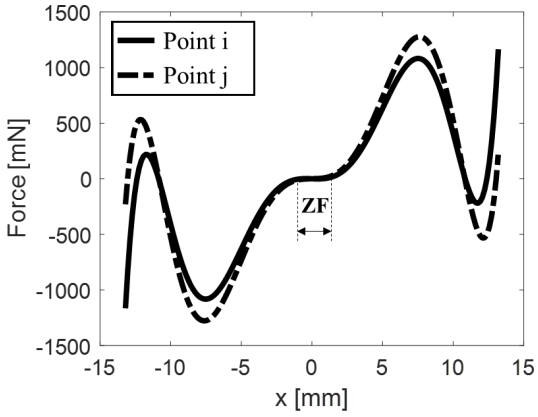

FIGURE 11. The reaction force of the mechanism programmed as ZFTM, the zero force (ZF) region is highlighted.

For $p_2^a > p_2$, the mechanism is always monostable with a stable state q_0 at $x = 0$. As $p_2^a < p_2$, the mechanism exhibits bistability. A pitchfork bifurcation occurs, the stable state q_0 becomes unstable and bifurcates into two stable states, $q_3^{\pm}$. At $p_2^a = p_2$, a saddle-node bifurcation of the zero stiffness positions occurs as well at $x = 0$ at which the mechanism exhibits zero force regime leading to ZFMM, as illustrated in Figure 12(a).

As p_2 increases two saddle-node bifurcations of the equilibrium states occur at which states $q_2^{\pm}$, $q_3^{\pm}$ appear. Zero stiffness positions appear at $p_1 = p_1^z$ at which the mechanism exhibits near constant force region, leading to CFMM. As p_1 increases, the zero stiffness positions merge at $x = 0$, at which zero force regime occurs resulting in ZFBM, as given in Figure 12(b). It should be noted that zero stiffness bifurcations occur at lower values of p_1 compared to equilibrium bifurcations, i.e., $p_1^z < p_1^{cr}$. On increasing p_2, the zero stiffness positions move apart from $x = 0$ and p_1^z decreases, as illustrated in Figure 12(c).

If $p_2^c < p_2$, bistability occurs and an inverted pitchfork bifurcation appears at which the unstable state q_0 becomes stable and the equilibrium states $q_1^{\pm}$ merge. A saddle-node bifurcation of the zero stiffness positions occurs as well at $x = 0$ at which the mechanism exhibits zero force response given in Figure 12(d).

On increasing p_2, p_2^c increases and p_1^z decreases until the near constant force regime appears within the bistable regime leading to CFBM, as illustrated in Figure 12(e).

On further increase of p_2, the mechanism exhibits zero stiffness regime at $x = 0$ within the tristable regime, leading to ZFTM, as illustrated in Figure 12(f).

5.2 Sweeping p_2 and fixing p_1

Figure 13 illustrates the variations of the zero stiffness and equilibrium positions as a function of p_2 for different values of

p_1. On selecting $p_1 < p_1^z$, the mechanism is monostable for $p_2 < p_2^c$ with a stable state q_0. Once p_2 exceeds p_2^c, the mechanism becomes bistable. A pitch-fork bifurcation occurs at $p_2 = p_2^c$ at which the stable state q_0 becomes unstable and bifurcates into two stable states. A saddle-node bifurcation of zero stiffness state occurs also at $p_2 = p_2^c$ at which the mechanism is ZFMM around $x = 0$, as illustrated in Figure 13(a).

On increasing p_1 such that $p_1 > p_1^z$ for a given range of p_2, two saddle-node bifurcations of zero stiffness positions occur. The mechanism exhibits constant force regime within the bistability region leading to CFBM, as given in Figure 13(b).

For higher values of p_1, the mechanism exhibits constant force regime within the monostable region leading to CFMM, as illustrated in Figure 13(c).

At $p_1 > p_1^{cr}$, the mechanism can exhibit monostability, bistability, tristability and quadrastability as illustrated in Figure 13(d). The zero stiffness states merge and the mechanism has zero stiffness response around $p_2 = p_2^a, p_2^b, p_2^c$ resulting in ZFMM, ZFBM and ZFTM respectively. The near zero force regions exist only around $x = 0$. The near constant force region appears at $p_1 = p_1^z$ and its position varies with p_2. The higher p_2 is, the lower p_1^z becomes.

6 Model verification

6.1 Finite element analysis

We used COMSOL FEM to verify our analysis. Our model is built using the solid mechanics module and geometric nonlinearity is considered in the model. Mesh converge test is performed to ensure the validity of the solution. We used the displacement driven method as it is a single-valued problem and easier to converge. On applying a given displacement to the central block of module 2 of the mechanism, the total strain energy is calculated and the reaction force is estimated.

6.2 Experimental setup

A prototype of the T-mechanism is manufactured using electro-discharge machining as illustrated in Figure 4(a) with the dimensions given in Table 3. Figure 14 gives the measurement setup of the mechanism [19]. It consists of three laser sensors to measure the displacement x, p_1, p_2 with a resolution down to $50[nm]$. A Kistler force sensor is used to measure the reaction force of the mechanism with a sensitivity of $5[mN]$. The actuation input is applied via a micrometric screw mounted on a stage connected to the actuation block of the T-mechanism by a nylon wire. A known mass is used to compensate for the negative stiffness of the mechanism. The programming inputs are applied via micrometric screws.

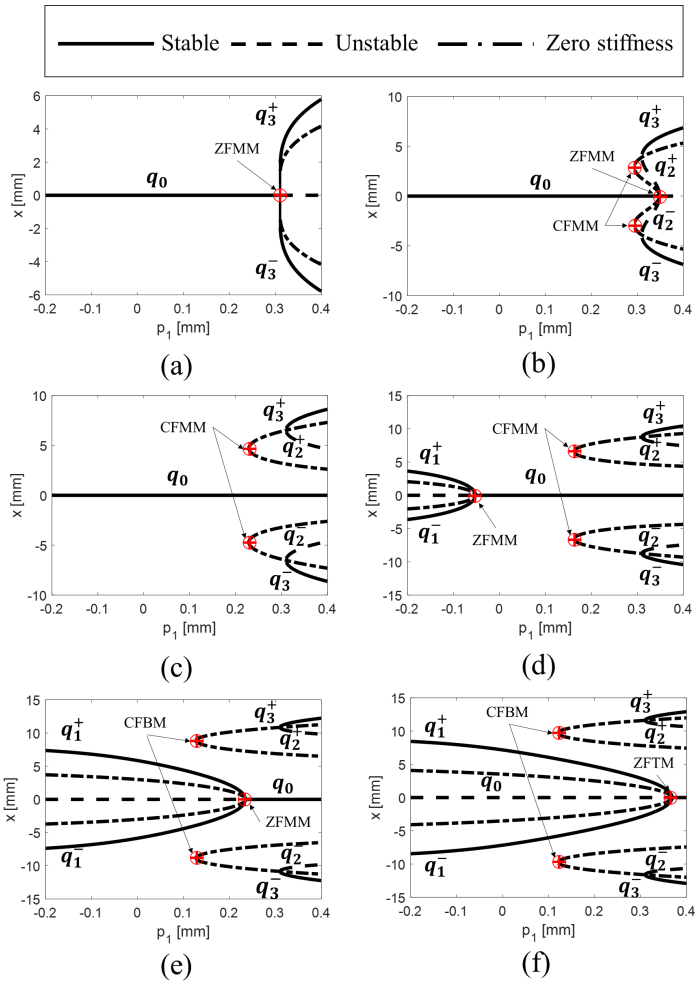

FIGURE 12. Bifurcation diagrams of zero stiffness and equilibrium states on sweeping p_1 for (a) $p_2 = -1.2[mm]$, (b) $p_2 = -0.8[mm]$, (c) $p_2 = 0[mm]$, (d) $p_2 = 1.0[mm]$, (e) $p_2 = 2.2[mm]$, (f) $p_2 = 2.7[mm]$.

6.3 Results

Figure 15 gives the reaction force of the mechanism calculated analytically, numerically and experimentally as ZFMM, CFMM, ZFBM, CFBM, ZFTM. A good match is found with a discrepancy of less than 10% due to neglecting higher order stiffness terms of the mechanism in our analytical model and measurement errors. We find the analytical model sufficient for the estimation of the reaction force of the mechanism and the validation of the constant force behavior of PMMs.

7 Applications

We applied programmable multistable mechanisms to retinal vein cannulation needles where the puncturing force and stroke are controlled to avoid vein double puncturing

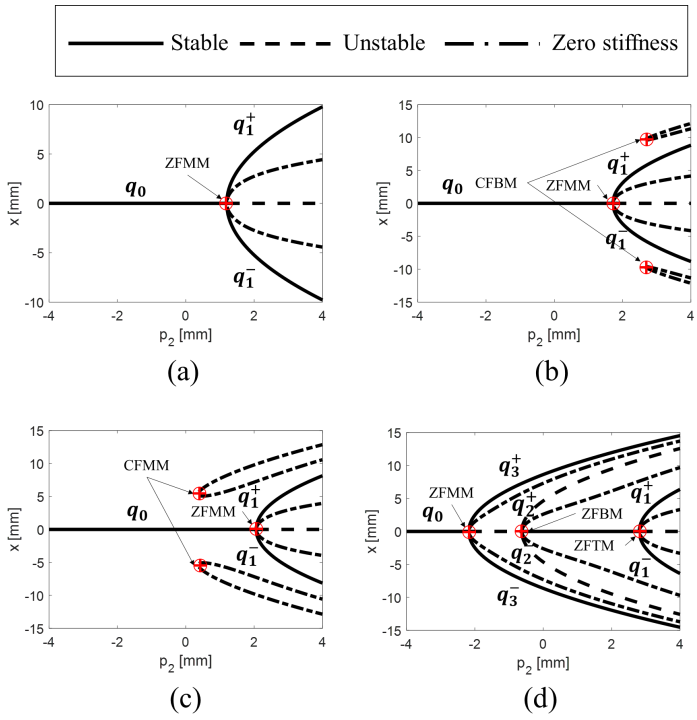

FIGURE 13. Bifurcation diagrams of zero stiffness and equilibrium states on sweeping p_2 for (a) $p_1 = 0.0[mm]$, (b) $p_1 = 0.12[mm]$, (c)$p_1 = 0.2[mm]$, (d) $p_1 = 0.4[mm]$.

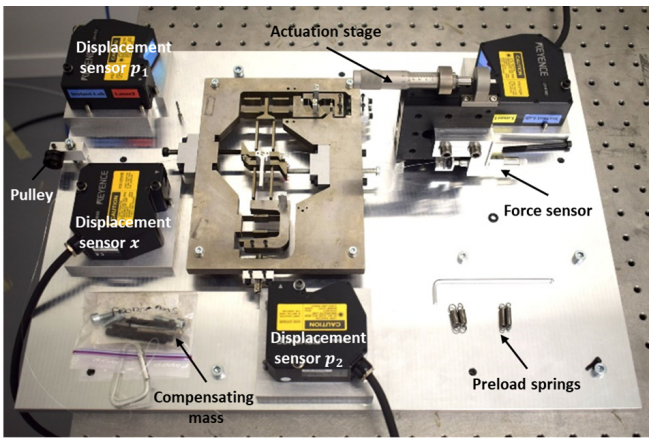

FIGURE 14. Measurement setup of the T-mechanism.

[20]. Other potential applications are micro-computing, programmable threshold sensors and force regulators, which is the focus of our current work.

8 Summary

We reported the zero stiffness behavior of the programmable T-shaped multistable mechanisms. We illustrated that the mechanism can be programmed as zero force monostable, constant force monostable, zero force bistable, constant force bistable and zero force tristable. Based on Euler-Bernoulli beam theory, the reaction force and tangential stiffness were derived, from which the stability and stiffness behaviors were characterized. Finite element analysis and experimental measurements were conducted to verify our analytical model and a discrepancy of less than 10% was found. Finally, we discussed possible applications of programmable stiffness mechanisms.

REFERENCES

[1] Herder, J., 2001. "Free energy system: Theory. conception and design of statically balanced spring mechanisms". PhD thesis, Delft University of Technology.

[2] Howell, L. L., 2001. *Compliant mechanisms*. John Wiley & Sons.

[3] Wang, P., and Xu, Q., 2018. "Design and modeling of constant-force mechanisms: A survey". *Mechanism and Machine Theory,* **119**, pp. 1–21.

[4] Liu, Y., Li, D.-J., Yu, D.-p., Miao, J.-g., and Yao, J., 2017. "Design of a curved surface constant force mechanism". *Mechanics Based Design of Structures and Machines,* **45**(2), pp. 160–172.

[5] Hou, C.-W., and Lan, C.-C., 2013. "Functional joint mechanisms with constant-torque outputs". *Mechanism and Machine Theory,* **62**, pp. 166–181.

[6] Jutte, C. V., and Kota, S., 2008. "Design of nonlinear springs for prescribed load-displacement functions". *Journal of Mechanical Design,* **130**(8), p. 081403.

[7] Morsch, F. M., and Herder, J. L., 2010. "Design of a generic zero stiffness compliant joint". In ASME 2010 International Design Engineering Technical Conferences and Computers and Information in Engineering Conference, American Society of Mechanical Engineers, pp. 427–435.

[8] Merriam, E. G., Colton, M., Magleby, S., and Howell, L. L., 2013. "The design of a fully compliant statically balanced mechanism". In Proceedings of ASME 2013 International Design Engineering Technical Conferences & Computers and Information in Engineering Conference, ASME, Vol. 5.

[9] Oh, Y., 2008. *Synthesis of multistable equilibrium compliant mechanisms*. PhD thesis, Umich.

[10] Chen, G., Gou, Y., and Zhang, A., 2011. "Synthesis of compliant multistable mechanisms through use of a single bistable mechanism". *Journal of Mechanical Design,* **133**(8), p. 081007.

[11] Chen, G., and Du, Y., 2013. "Double-young tristable mechanisms". *Journal of Mechanisms and Robotics,* **5**(1), p. 011007.

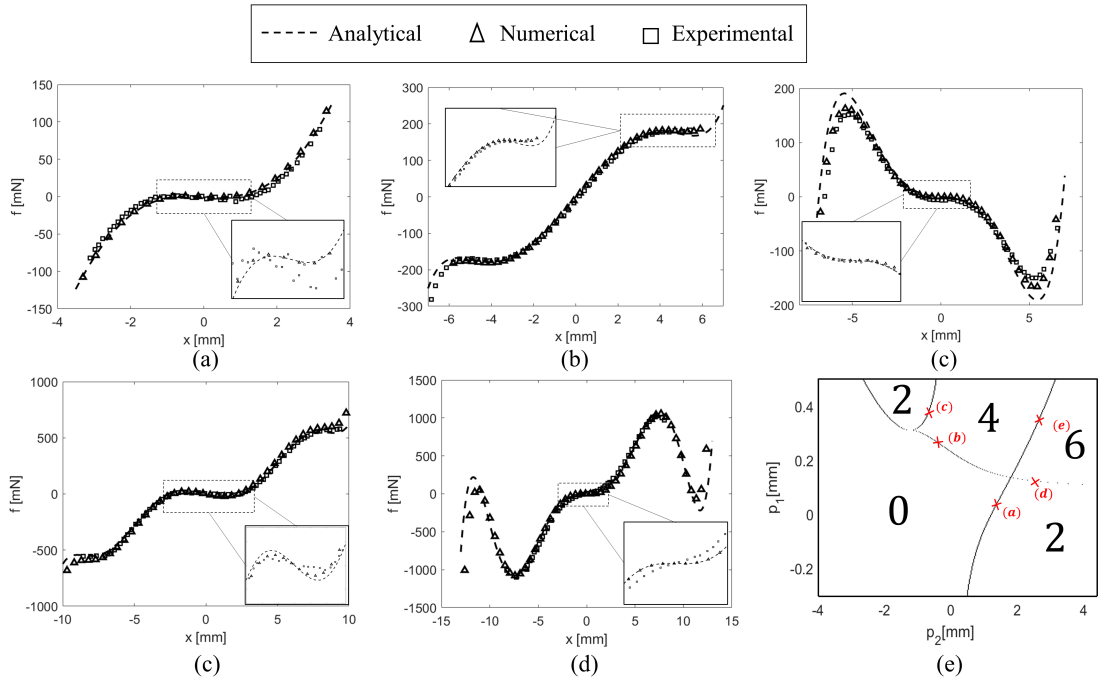

FIGURE 15. Reaction force of the T-mechanism based on analytical, numerical and experimental measurements for (a) ZFMM at $p_1 = 0.09[mm]$, $p_2 = 1.6[mm]$, (b) CFMM at $p_1 = 0.24[mm]$, $p_2 = 0.0[mm]$, (c) ZFBM at $p_1 = 0.39[mm]$, $p_2 = -0.7[mm]$, (d) CFBM at $p_1 = 0.14[mm]$, $p_2 = 2[mm]$, (e) ZFTM at $p_1 = 0.35[mm]$, $p_2 = 2.65[mm]$, (f) selected points highlighted along the zero stiffness boundaries.

[12] Oberhammer, J., Tang, M., Liu, A.-Q., and Stemme, G., 2006. "Mechanically tri-stable, true single-pole-double-throw (SPDT) switches". *Journal of Micromechanics and Microengineering,* **16**(11), p. 2251.

[13] Harne, R., and Wang, K., 2013. "A review of the recent research on vibration energy harvesting via bistable systems". *Smart Materials and Structures,* **22**(2), p. 023001.

[14] Wang, D.-A., Chen, J.-H., and Pham, H.-T., 2013. "A constant-force bistable micromechanism". *Sensors and Actuators A: Physical,* **189**, pp. 481–487.

[15] Zanaty, M., 2018. "Programmable multistable mechanisms". PhD thesis, Ecole polytechnique federale de Lausanne.

[16] Zanaty, M., Vardi, I., and Henein, S., 2018. "Programmable multistable mechanisms: Synthesis and modeling". *Journal of Mechanical Design,* **140**(4), p. 042301.

[17] Chen, G., Aten, Q. T., Zirbel, S., Jensen, B. D., and Howell, L. L., 2010. "A tristable mechanism configuration employing orthogonal compliant mechanisms". *Journal of Mechanisms and Robotics,* **2**(1), p. 014501.

[18] Awtar, S., Slocum, A. H., and Sevincer, E., 2007. "Characteristics of beam-based flexure modules". *Journal of Mechanical Design,* **129**(6), pp. 625–639.

[19] Zanaty, M., and Henein, S., 2018. "Experimental characterization of a t-shaped programmable multistable mechanism". *ASME Journal of Mechanical Design, DOI: 10.1115/1.4040173*.

[20] Zanaty, M., Rogg, A., Fussinger, T., Lovera, A., Baur, C., Bellouard, Y., and Henein, S., 2017. "Safe puncture tool for retinal vein cannulation". In Proceeding of Design of medical devices (DMD).